Investigation of Effects of Process Variables on Weld Bead Characteristics in Surface Coating of 309L Stainless Steel by Wire Arc Additive Manufacturing

Van Thuc Dang[1], Van Thao Le[1,*], Trung Thanh Nguyen[2], Van Luu Dao[1]

[1]Advanced Technology Center, Le Quy Don Technical University, Hanoi, Viet Nam

[2]Faculty of Mechanical Engineering, Le Quy Don Technical University, Hanoi, Viet Nam

Received 29 August 2024; received in revised form 15 October 2024; accepted 17 October 2024

DOI: https://doi.org/10.46604/aiti.2024.14208

Abstract

Coating carbon steel surfaces with stainless steel is a crucial technology in various industries to extend the product lifespan. This study focuses on investigating the effects of process parameters on weld bead characteristics in coating SS309L on carbon steel substrates by wire arc additive manufacturing (WAAM) and identifying the optimal parameters. The key parameters are current, travel speed, and voltage, while the weld bead characteristics include height, width, and depth of penetration. Experimental data and analysis of variance (ANOVA) are employed to develop and evaluate predictive models in Minitab software. The results show that the optimal process parameters for coating SS309L on carbon steel substrates by WAAM are voltage = 22 V, current = 132 A, and travel speed = 0.3 m/min, which improve height and width by 56.71% and 25.87%, respectively, while reducing the depth of penetration by 21.74% compared to the worst-case scenario.

Keywords: WAAM, surface coating, 309L stainless steel, optimization

1. Introduction

Stainless steels are commonly used for components that need to withstand corrosive environments due to their excellent resistance to rust and corrosion. However, stainless steel is much more expensive than carbon steel, making it especially costly for parts with large structural dimensions. To reduce material costs, stainless steel is often applied as a coating on carbon steel components used in various industries, including nuclear applications [1], petrochemical industries [2], and desalination processes [3]. This approach not only maintains the desired properties of stainless steel in the outer layer but also leverages the cost-effectiveness and strength of carbon steel as the core material. Additionally, the use of stainless-steel coatings can extend the lifespan of carbon steel components, reduce maintenance costs, and enhance overall performance in harsh environments.

Wire arc additive manufacturing (WAAM) is a metal 3D printing technology, which utilizes a welding arc source to melt the metal wire and form a 3D physical part layer-by-layer. This method offers a promising approach for producing medium to large-sized metal parts or coating and repairing applications. WAAM provides an elevated rate of material deposition (4-8 kg/h) and lower equipment investment costs compared to other metal 3D printing technologies [4]. In WAAM, the arc source can be Gas Metal Arc Welding (GMAW), Plasma Arc Welding (PAW), or Gas Tungsten Arc Welding (GTAW). Among these, the WAAM process using GMAW has a deposition rate two to three times higher than that using GTAW and PAW [5]. Therefore, the WAAM process using a GMAW source is more suitable for manufacturing large-dimensional parts.

* Corresponding author. E-mail address: vtle@lqdtu.edu.vn

English language proofreader: Chih-Wen Teng

In the WAAM process, the metal wire is melted and deposited onto a substrate surface following a toolpath to create weld beads, which serve as the fundamental geometric unit for building a part [6]. Parts can be constructed by depositing multiple single beads layer by layer (e.g., for thin walls) [7] or by depositing successive layers with overlapping beads (e.g., thick walls) [8]. The shape and quality of a weld bead, such as smoothness and stable form, significantly affect the process stability, and the external and internal quality of the finished parts. The key geometric attributes of weld beads, including the width (W_{wb}), height (H_{wb}), and depth of penetration (D_{wb}) - are critical for generating toolpaths. Consequently, many studies have focused on predicting weld bead geometries for the WAAM process. Xiong et al. [9] proposed prediction models for the height and width of weld beads in WAAM of low-carbon steels. They suggested that these models, which offer adequate accuracy, could be used to estimate the size of weld beads for model slicing and toolpath planning.

Le et al. [10] estimated the optimal parameters for WAAM of 0.35Cr1.9Ni0.55Mo steels. The part fabricated using the optimal parameters is free of defects, demonstrating their effectiveness. Suryakumar et al. [11] developed and validated W_{wb} and H_{wb} models for low-carbon steels based on experimental data. They proved that these models could predict and optimize process variables for both additive and subtractive manufacturing processes. Kumar and Maji [12] predicted weld bead characteristics in the WAAM of SS304L, using the Desirability approach (DA) to estimate optimal variables. Youheng et al. [13] also estimated optimal parameters for WAAM of bainite steel using DA available in Minitab software. Sarathchandra et al. [14] examined the influence of process parameters on weld bead geometries of SS304 produced by WAAM. They employed the response surface methodology (RSM) to identify optimal input variables.

Concerning surface coating, Switzner and Yu [2] coated austenitic stainless steel onto low-carbon steel using three different processes: fusion welding, hot roll bonding, and inertia friction welding. In this study, the interfaces of claddings made by three different processes were compared regarding the microhardness, composition, phase, morphology, and etching response. Pravin Kumar et al. [15] studied the microstructure and electrochemical corrosion behavior of SS308L coating on the surface of SS AISI 321 using Robotic-GMAW for repair applications. Recently, Bozeman et al. [16] clad SS309L wire onto carbon steel substrates using laser-wire directed energy deposition. They examined the effects of processing parameters (laser power and travel speed) on metallurgical bonding and microstructures. Cracking, stubbing, and delamination flaws are associated with insufficient heat input while wire dripping problems are associated with excessive heat input.

Although research has been performed on the surface coating of stainless steels on carbon steel substrates, as mentioned above, a systematic investigation on the influence of process parameters on weld bead characteristics in the coating of SS309L applied to carbon steel surfaces by WAAM has not reported yet. Therefore, the objectives of this study are twofold:

(1) Exploring the effects of WAAM parameters for coating SS309L on carbon steel plates
(2) Identifying the proper parameters to ensure the deposition of a weld bead with maximal W_{wb}, maximal H_{wb}, and minimal D_{wb}

To achieve these goals, the analysis of variance (ANOVA) is used to identify the significance of individual process parameters and their interactions with the quality of the coating. ANOVA helps in understanding the contribution of each parameter to the overall performance, thereby guiding the optimization process. The desirable function method, which provides a robust framework for parameter optimization, is used to identify the proper process parameters.

2. Experimental Methodology

In this section, the raw materials and the WAAM system used in the study are first presented. Subsequently, the experiment method is introduced. The experiments include two steps:

(1) Determining the range of process parameters
(2) Designing of experiment and collecting data for the mode development

2.1. Materials

SS309L is an austenitic stainless steel, notable for its excellent corrosion resistance and high-temperature resistance. JIS G 3101 carbon steel is a popular structural material due to its high mechanical strength and low cost. The coating of SS309L on the surface of carbon steel enhances the corrosion resistance of the carbon steel plate. In this study, experiments were performed using SS309L welding wire with a diameter of 1.2 mm and JIS G 3101 steel plates with a size of 200 mm in length, 200 mm in width, and 10 mm in thickness. The chemical compositions of SS309L welding wire and JIS G 3101 steel substrate are detailed in Table 1. The WAAM system consists of a Panasonic TA-1400 welding robot arm equipped with a GMAW power source (Fig. 1). Argon gas with a purity of 99.99% and a flow rate of 16 L/min was employed to protect the molten metal during the deposition.

Table 1 Chemical elements of SS309L and JIS G 3101 steel (in wt.%)

Materials	Mn	Ni	Cr	Mo	Si	C	P	S	Fe
SS309L wire	2	14	23	0.05	1	0.02	-	-	Balanced
JIS G 3101 steel plate	<5	-	-	-	<5	-	-	-	Balanced

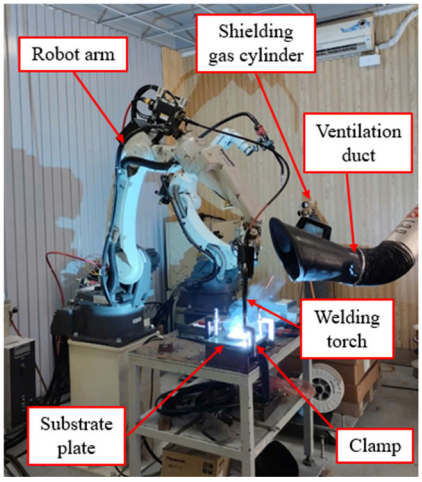

Fig. 1 The WAAM robot system

2.2. Experiment procedure and data collection

The experiment was conducted through the steps below:

Step 1: Determining the range of process parameters: To establish the upper and lower limits of each input process parameter, several experimental runs were conducted to produce single weld beads. The parameter levels were chosen based on the recommended ranges provided by suppliers for traditional welding processes. Specifically, the welding current (I) ranged from 100-160 A, the voltage (U) was adjusted between 16 V and 25 V, and the travel speed (v) varied from 0.3-0.6 m/min. These experiments were conducted in the previous study [17]. After analyzing the effects of process parameters on the geometric characteristics of the single weld bead (Fig. 2), the following ranges were identified as suitable for metal deposition applications: I = 120-150 A, v = 0.3-0.45 m/min, and U = 19-22 V. These settings enable the production of continuous weld beads with minimal spatter.

Step 2: Experiment design and data collection: The study focused on three process parameters: U, I, and v as these factors significantly affect the weld beads' characteristics. Each parameter was tested at four different levels (see Table 2). The experiment campaign was created using the Taguchi-L16 method. The Taguchi method in experimental design offers several advantages, such as saving time and costs using orthogonal arrays, allowing for quick optimization of factors affecting product quality. It is also easy to apply, helping to improve the reliability and quality of products by creating designs that are less sensitive to variations. Consequently, 16 experimental runs were conducted (Table 3).

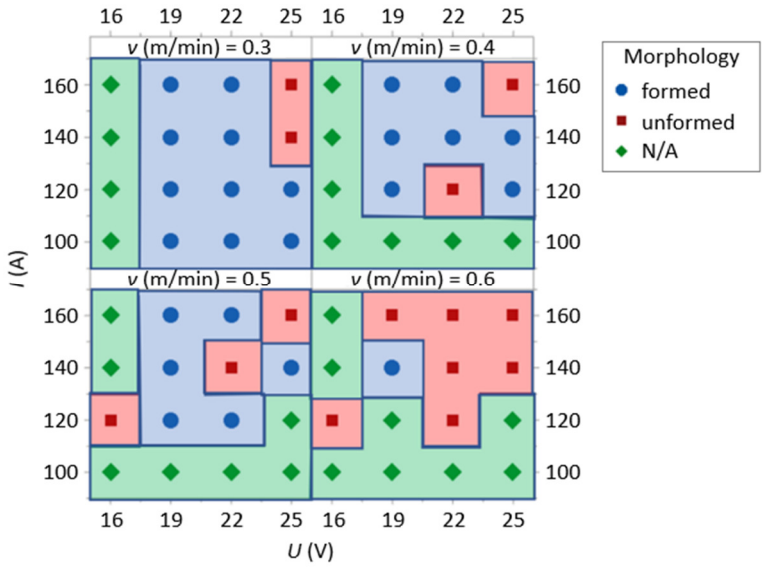

Fig. 2 The process parameter window for the weld bead morphology [17]

Table 2 Input parameters and its levels

Input parameters	Level 1	Level 2	Level 3	Level 4
I (A)	120	130	140	150
U (V)	19	20	21	22
v (m/min)	0.3	0.35	0.4	0.45

Table 3 Experiment results

Exp. runs	Process parameters			Attributes		
	U (V)	I (A)	v (m/min)	W_{wb} (mm)	H_{wb} (mm)	D_{wb} (mm)
1	19	120	0.30	4.04±0.08	2.36±0.10	0.48
2	19	130	0.35	4.13±0.08	2.28±0.09	0.65
3	19	140	0.40	4.28±0.05	2.22±0.04	0.74
4	19	150	0.45	3.98±0.09	2.39±0.12	0.72
5	20	120	0.35	4.32±0.06	2.18±0.08	0.62
6	20	130	0.30	4.56±0.10	2.48±0.07	0.59
7	20	140	0.45	4.14±0.06	1.95±0.08	0.64
8	20	150	0.40	4.42±0.05	2.34±0.05	0.75
9	21	120	0.40	4.22±0.06	2.08±0.07	0.63
10	21	130	0.45	4.34±0.11	1.80±0.09	0.58
11	21	140	0.30	5.33±0.10	2.53±0.07	0.73
12	21	150	0.35	4.96±0.05	2.33±0.13	0.88
13	22	120	0.45	4.02±0.06	1.64±0.06	0.69
14	22	130	0.40	4.33±0.11	1.98±0.07	0.52
15	22	140	0.35	4.74±0.16	2.23±0.11	0.59
16	22	150	0.30	5.76±0.09	2.40±0.12	0.99

After fabricating the weld bead samples, the characteristics (W_{wb}, H_{wb}, and D_{wb}) were measured (see Fig. 3). They are critical in the WAAM process. Measurements were taken in the weld beads' stable zone (Fig. 4) using a digital caliper, which features 0.01 mm and ±0.02 mm in resolution and accuracy, respectively. For W_{wb} and H_{wb}, to address measurement uncertainties, five measurements were performed at five positions in the stable region of the weld beads, as described in Fig. 4, and the mean of the measured results was calculated for analysis. Meanwhile, D_{wb} was determined from optical images of the weld bead cross-sections captured by an optical microscope (Fig. 5). The results from the experiment and the measured data are presented in Table 3. The standard deviation errors of the mean values for W_{wb} and H_{wb} are presented in Table 3. These errors indicate the inherent variability of the weld in practical applications. In this case, the deviations are around ± 0.10 mm, indicating the high accuracy and reliability of measured data.

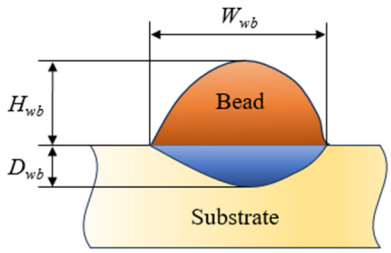

Fig. 3 The geometric parameters of the single weld

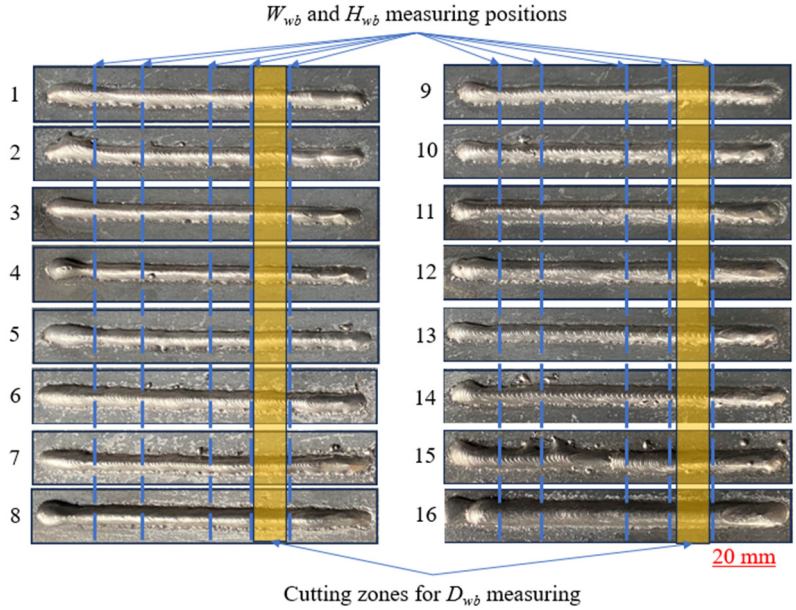

Fig. 4 Sixteen single weld lines

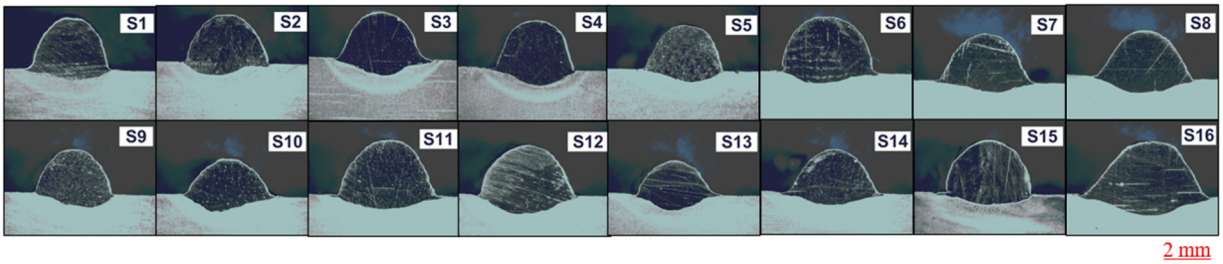

Fig. 5 Cross section of the welding beads

2.3. Optimization method

To assess the influence of process parameters and their contribution to each characteristic, ANOVA in Minitab software was utilized. This statistical analysis was performed with 95% confidence and 5% significance. For multi-objective optimization problems, desirability function (DF) and RSM are two popular approaches, particularly in the context of experimental design and process improvement. The DF method allows for the simultaneous optimization of multiple conflicting objectives, while RSM often requires data to follow complex regression models (e.g., quadratic polynomial models), which may not be suitable in all cases. Moreover, once the regression models are developed by RSM, DF can be used to identify the optimal process parameters. Therefore, the DF method was adopted in this study.

In the case of surface coating by WAAM, the goal is to maximize W_{wb} and H_{wb} while minimizing D_{wb} to improve productivity and reduce the heat-affected zone in the substrate material. The criteria for optimization are described below:

$$\begin{aligned} &\text{Find } X = \{U, I, v\} \text{ that } maximizing\{W_{wb} \text{ and } H_{wb}\} \text{ while } minimizing\{D_{wb}\} \\ &\text{Subject to } U(\text{V}) \in [19;22];\ I(\text{A}) \in [120;150];\ v(\text{m/min}) \in [0.3;1.45] \end{aligned} \tag{1}$$

The DF approach is described as follows: each response R_i is transformed into a desirability index DF_i, within the range of [0, 1], depending on whether R_i is beneficial or costly. The corresponding equations for both types of responses are provided below.

$$DF_i(R_i) = \begin{cases} 0, R_i \in (-\infty, Min) \\ \left(\dfrac{R_i - Min}{Max - Min}\right)^r, R_i \in (Min, Max) \\ 1, R_i \in (Max, +\infty) \end{cases} \tag{2}$$

$$DF_i(R_i) = \begin{cases} 0, R_i \in (-\infty, Min) \\ \left(\dfrac{Max - R_i}{Max - Min}\right)^r, R_i \in (Min, Max) \\ 1, R_i \in (Max, +\infty) \end{cases} \tag{3}$$

where $Min = min(R_i)$, $Max = max(R_i)$, and r indicates the form factor of DF_i. Finally, the DF is calculated by:

$$DF = \left(\prod_{i=1}^{M} DF_i^{w_i}\right)^{1/\sum_{i=1}^{M} w_i} \tag{4}$$

where w_i signifies the weight of the i-th response, and M is the number of responses. Herein, the value of r is equal to 1, and the weight for each response is set equally, $w_1 = w_2 = w_3 = 1/3$.

Taking a calculation example based on the data given in Table 3, Max(W_{wb}) = 5.76 mm, Min(W_{wb}) = 3.98 mm, Max(H_{wb}) = 2.53 mm, Min(H_{wb}) = 1.64 mm, Max(D_{wb}) = 0.99 mm, Min(D_{wb}) = 0.48 mm. In this study, W_{wb} and H_{wb} are the beneficial responses, while D_{wb} is the costly response. As a result, for Run #1, $DF_1(W_{wb})$ = (4.04 − 3.98) / (5.78 − 3.98) = 0.0333 $DF_1(H_{wb})$ = (2.36 − 1.64) / (2.53 − 1.64) = 0.8090, and $DF_1(D_{wb})$ = (0.99 − 0.48) / (0.99 − 0.48) = 1. Finally, the DF corresponding to Run #1 is calculated as: DF(#1) = $(0.0337 \times 0.8090 \times 1)^{1/3}$ = 0.0091.

3. Results and Discussion

In this section, the results of the model development are first presented. The evaluation of the developed model with ANOVA results is also introduced. Thereafter, the effects of process parameters on the weld bead characteristics are discussed. Lastly, the results of the optimization problem are presented with a comparison with the worst case.

3.1. ANOVA results for the developed models

The developed models of W_{wb}, H_{wb}, and D_{wb} are described by the following formulas, respectively. These models were developed using Minitab software.

$$\begin{aligned} W_{wb} = {} & -43.5 + 3.03 \times U + 0.063 \times I + 63.5 \times v \\ & + 0.00382 \times U \times I - 2.126 \times U \times v - 0.2901 \times I \times v \\ & - 0.0649 \times U \times U - 0.000074 \times I \times I + 19.5 \times v \times v \end{aligned} \tag{5}$$

$$\begin{aligned} H_{wb} = {} & -20.01 + 1.707 \times U + 0.0732 \times I + 3.30 \times v \\ & - 0.00691 \times U \times I - 0.876 \times U \times v + 0.0865 \times I \times v \\ & - 0.0119 \times U \times U + 0.000156 \times I \times I - 1.95 \times v \times v \end{aligned} \tag{6}$$

$$\begin{aligned} D_{wb} = {} & -4.67 + 0.230 \times U - 0.0407 \times I + 31.84 \times v \\ & - 0.000295 \times U \times I - 0.40 \times U \times v - 0.1832 \times I \times v \\ & - 0.0025 \times U \times U + 0.000450 \times I \times I + 1.00 \times v \times v \end{aligned} \tag{7}$$

The P-values in the regression model enable the identification of significant and insignificant terms of the model. If the P-value <0.05, the model and the model terms are considered significant. On the other hand, a P-value >0.05 indicates insignificant terms. For determination coefficients of the models, R-squared (R-sq) is used to assess the fit of the model to the data. A higher R-sq value indicates that the model explains the variability in the data better. However, a high R-sq value does not always mean the regression model is valid. Adding variables, whether statistically significant or not, will always increase the R-sq value. In other words, a model with a high R-sq value might still perform poorly in predicting new data or estimating the average response.

Therefore, the adjusted R-squared (R-sq(adj)), a modified version of R-sq that accounts for the number of predictors in the model, is preferred. Unlike R-sq, the R-sq(adj) can decrease if new variables do not improve the model significantly. This makes it a more reliable metric for comparing models with different numbers of predictors. Moreover, if the predicted R-squared (R-sq(pred)) is in reasonable agreement with the R-sq(adj), i.e., their difference is less than 0.2, this suggests that the model maintains a good balance between predictive accuracy and the adjustment for the number of predictors, thereby reinforcing the reliability of the results.

For the W_{wb} model (Eq. (5) and Table 4), the P-values of the model terms (v, U, $U \times v$, and $I \times v$) are less than 0.05, meaning that they are significant terms of the model. Meanwhile, the P-values of other model terms are bigger than 0.05, indicating they are not significant in the W_{wb} model. The R-sq, R-sq(adj), and R-sq(pred) values are 98.18%, 95.46%, and 87.73%, respectively demonstrating that the W_{wb} model has good accuracy and can reliably predict responses across the entire design space.

Table 4 ANOVA results for W_{wb}

Source	DF	Seq SS	Contribution	Adj SS	Adj MS	F-value	P-value
Regression	9	3.66586	98.18%	3.66586	0.407318	36.04	0.000
U (V)	1	0.93355	25.00%	0.06925	0.069245	6.13	0.048
I (A)	1	0.94135	25.21%	0.00391	0.003915	0.35	0.578
v (m/min)	1	1.38706	37.15%	0.12197	0.121967	10.79	0.017
$U \times I$	1	0.01284	0.34%	0.01284	0.012844	1.14	0.327
$U \times v$	1	0.09943	2.66%	0.09943	0.099429	8.80	0.025
$I \times v$	1	0.18519	4.96%	0.18519	0.185194	16.39	0.007
$U \times U$	1	0.06734	1.80%	0.06734	0.067340	5.96	0.050
$I \times I$	1	0.00087	0.02%	0.00087	0.000870	0.08	0.791
$v \times v$	1	0.03822	1.02%	0.03822	0.038220	3.38	0.116
Error	6	0.06780	1.82%	0.06780	0.011301	-	-
Total	15	3.73366	100.00%	-	-	-	-
R-sq = 98.18%			R-sq(adj) = 95.46%			R-sq(pred) = 87.73%	

For the H_{wb} model, as indicated in Eq. (6) and Table 5, the P-values for U, $U \times I$, $U \times v$, and $I \times v$ are less than 0.05, whereas the P-values for I and v are greater than 0.05. Thus, U, $U \times I$, $U \times v$, and $I \times v$ are identified as significant terms in the H_{wb} model. The coefficients R-sq, R-sq(pred), and R-sq(adj) are 98.30%, 82.68%, and 95.76%, respectively, demonstrating that the H_{wb} model has reasonable accuracy and is suitable for predicting responses throughout the entire design space.

Table 5 ANOVA results for H_{wb}

Source	DF	Seq SS	Contribution	Adj SS	Adj MS	F-value	P-value
Regression	9	0.921644	98.30%	0.921644	0.102405	38.63	0.000
U (V)	1	0.128160	13.67%	0.022030	0.022030	8.31	0.028
I (A)	1	0.201804	21.52%	0.005361	0.005361	2.02	0.205
v (m/min)	1	0.509762	54.37%	0.000330	0.000330	0.12	0.736
$U \times I$	1	0.042035	4.48%	0.042035	0.042035	15.86	0.007
$U \times v$	1	0.016879	1.80%	0.016879	0.016879	6.37	0.045

Table 5 ANOVA results for H_{wb} (continued)

Source	DF	Seq SS	Contribution	Adj SS	Adj MS	F-value	P-value
$I \times v$	1	0.016461	1.76%	0.016461	0.016461	6.21	0.047
$U \times U$	1	0.002256	0.24%	0.002256	0.002256	0.85	0.392
$I \times I$	1	0.003906	0.42%	0.003906	0.003906	1.47	0.270
$v \times v$	1	0.000380	0.04%	0.000380	0.000380	0.14	0.718
Error	6	0.015904	1.70%	0.015904	0.002651	-	-
Total	15	0.937548	100.00%	-	-	-	-
R-sq = 98.30%			R-sq(adj) = 95.76%			R-sq(pred) = 82.68%	

In the D_{wb} model, as shown in Eq. (7) and Table 6, the P-value for v is less than 0.05, while the P-values for U and I are greater than 0.05. This indicates that v is the significant factor in the model. The coefficients R-sq, R-sq(adj), and R-sq(pred) are 98.19%, 95.49%, and 86.29%, respectively, suggesting that the D_{wb} model has a high degree of accuracy and can reliably predict the responses throughout the entire design space.

Table 6 ANOVA results for *Dwb*

Source	DF	Seq SS	Contribution	Adj SS	Adj MS	F-value	P-value
Regression	9	0.244309	98.19%	0.244309	0.027145	36.27	0.000
U (V)	1	0.008405	13.02%	0.000401	0.000401	0.54	0.492
I (A)	1	0.121680	48.91%	0.001663	0.001663	2.22	0.187
v (m/min)	1	0.004205	1.69%	0.030650	0.030650	40.95	0.001
$U \times I$	1	0.000077	0.03%	0.000077	0.000077	0.10	0.760
$U \times v$	1	0.003520	1.41%	0.003520	0.003520	4.70	0.073
$I \times v$	1	0.073822	29.67%	0.073822	0.073822	98.63	0.000
$U \times U$	1	0.000100	0.04%	0.000100	0.000100	0.13	0.727
$I \times I$	1	0.032400	13.02%	0.032400	0.032400	43.29	0.001
$v \times v$	1	0.000100	0.04%	0.000100	0.000100	0.13	0.727
Error	6	0.004491	1.81%	0.004491	0.000748	-	-
Total	15	0.248800	100.00%	-	-	-	-
R-sq = 98.19%			R-sq(adj) = 95.49%			R-sq(pred) = 86.29%	

3.2. Correlation between process parameters and characteristics

Fig. 6(a) illustrates that W_{wb} increases as U and I are increased, whereas W_{wb} decreases with higher v. As indicated by the ANOVA results, v has the most significant influence on W_{wb}, contributing 37.15%, followed by the I with 25.21%, and U with 25.00% contribution. The influence of these parameters on W_{wb} can be explained as follows. Increasing the voltage results in a larger arc length and spread, which leads to a wider W_{wb} [14]. An increment in I boosts the wire feed speed and the amount of deposited material, leading to a larger molten pool and wider weld beads [18]. On the other hand, higher v decreases the quantity of deposited material per unit length, resulting in W_{wb} being narrower [14]. Fig. 6(b) to Fig. 6(d) show the interactive effects of process variables on W_{wb}. They reveal that W_{wb} increases with U across all values of I and v (Fig. 6(b) and Fig. 6(c)) and decreases with higher v for all values of U and I (Fig. 6(c) and Fig. 6(d)).

Fig. 7(a) presents the main effects of process parameters on H_{wb}. It is found that an increase in U and v leads to decreasing H_{wb}. On the other hand, H_{wb} increases when I augment. As indicated by the ANOVA results (Table 5), v has the most significant influence on W_{wb}, contributing 54.37%, followed by I with 21.52%, and U with 13.67% contribution. The amount of material deposited into the workpiece per length unit reduces when v increases. Therefore, H_{wb} decreases [14-19]. As U increases, the arc spreading zone becomes wider. As a result, the weld bead is flatter [20]. Hence, H_{wb} shows a decreasing tendency with the increase in U. On the other hand, when I increase, the wire feed speed increases. Thereby, the deposited material amount rises, thus H_{wb} also increases [14]. Fig. 7(b) to Fig. 7(d) show the interactive effects of process variables on H_{wb}. They reveal that H_{wb} increases when v decreases (Fig. 7(c) and Fig. 7(d)).

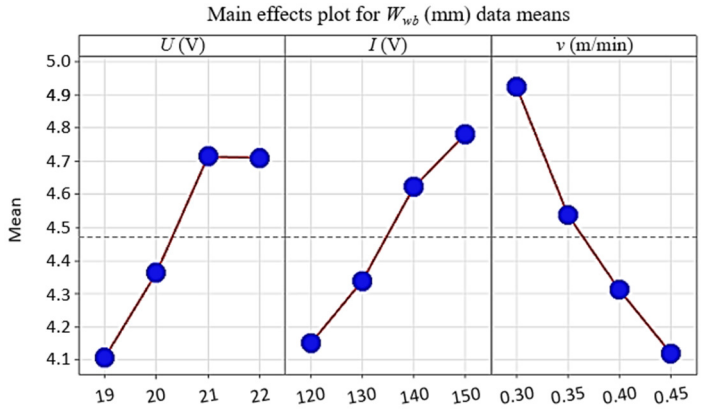

(a) Direct effects of process parameters on W_{wb}

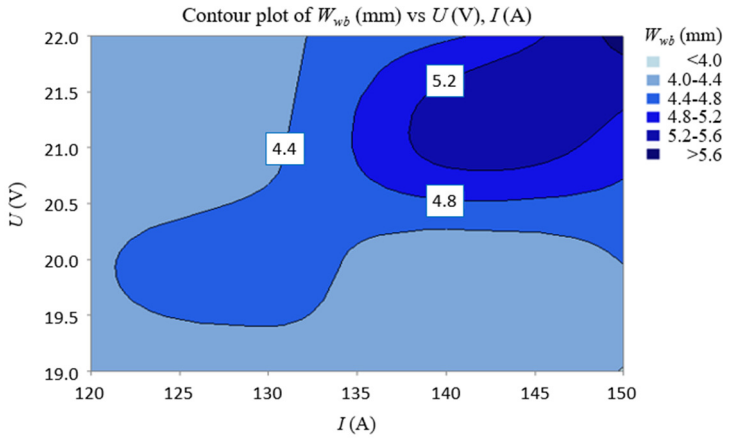

(b) Interactive effect of U, I on W_{wb}

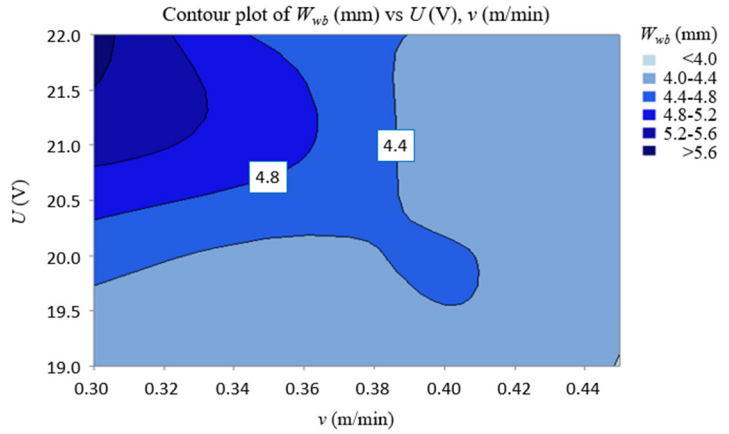

(c) Interactive effect of U, v on W_{wb}

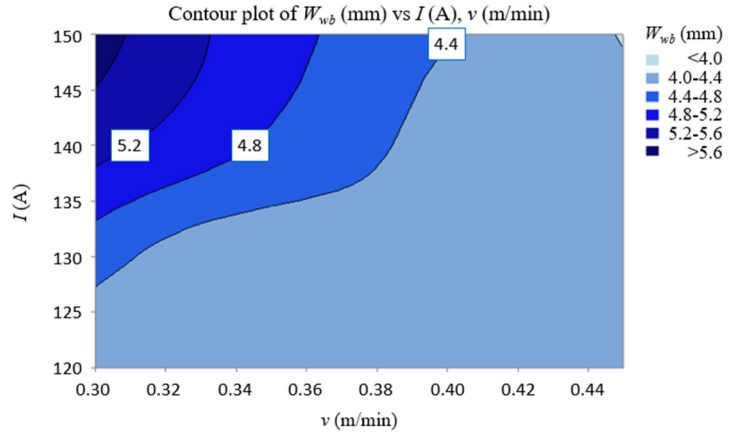

(d) Interactive effect of I, v on W_{wb}

Fig. 6 Direct and interactive impacts of process parameters on W_{wb}

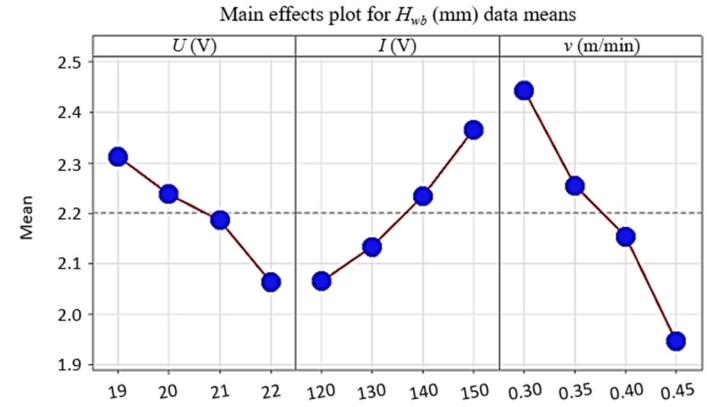

(a) Direct effects of process parameters on H_{wb}

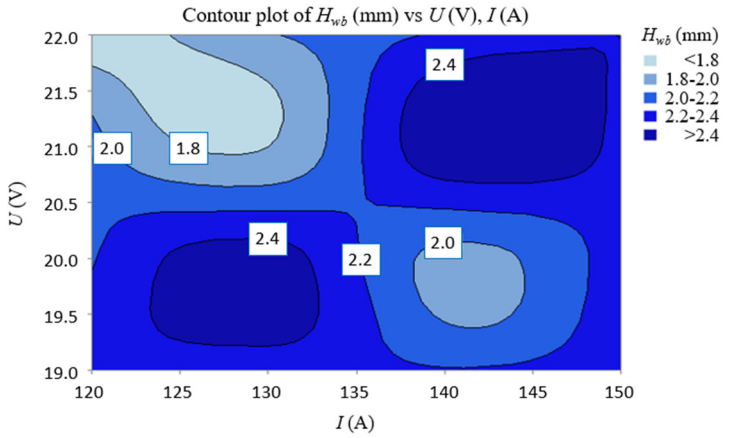

(b) Interactive effect of U, I on H_{wb}

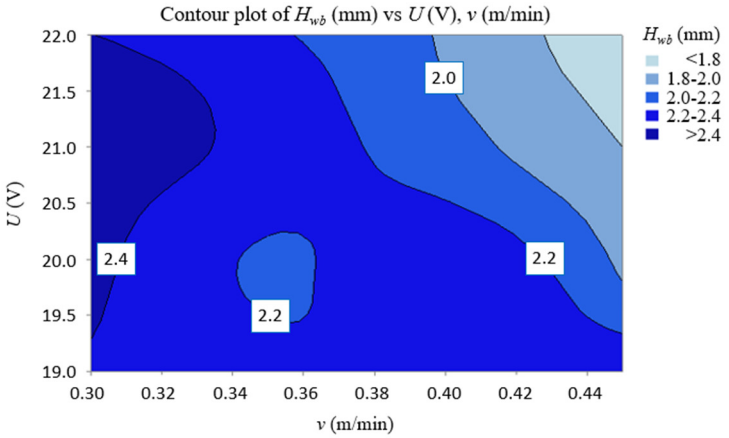

(c) Interactive effect of U, v on H_{wb}

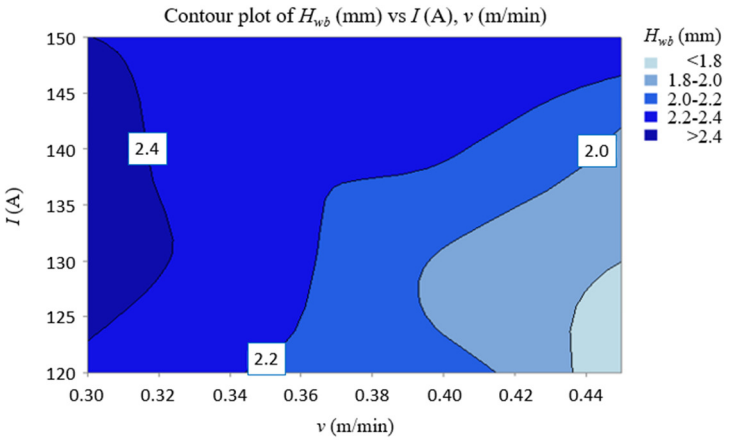

(d) Interactive effect of I, v on H_{wb}

Fig. 7 Direct and interactive impacts of process parameters on H_{wb}

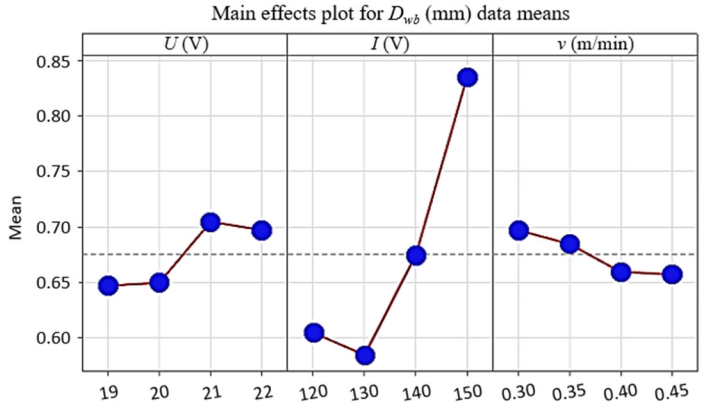

(a) Direct effects of process parameters on D_{wb}

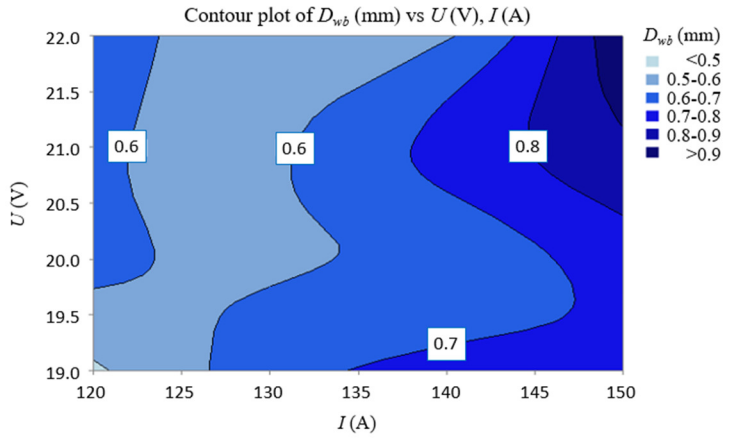

(b) Interactive effect of U, I on D_{wb}

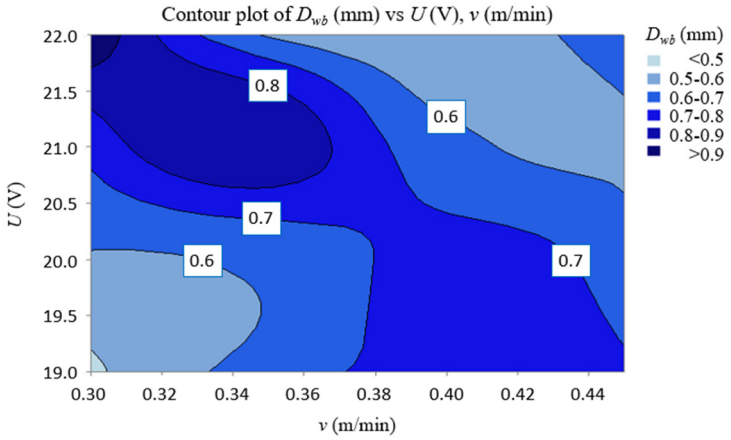

(c) Interactive effect of U, v on D_{wb}

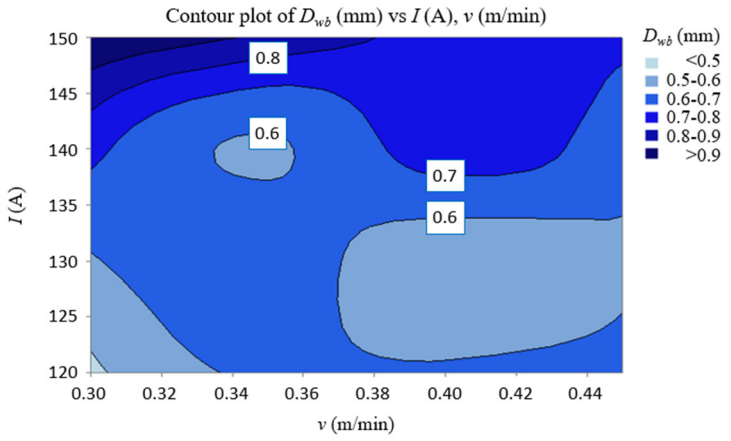

(d) Interactive effect of I, v on D_{wb}

Fig. 8 Direct and interactive impacts of process parameters on D_{wb}

For D_{wb}, as shown in Fig. 8(a), it decreases when the I increases from 120 A to 130 A. However, D_{wb} significantly increases as the current rises from 130 A to 150 A, with a slight increase in D_{wb} as the current continues to increase. Conversely, D_{wb} decreases as U and v increase. These observations are supported by the results of ANOVA (Table 6). It is indicated that I have the greatest impact on D_{wb}, contributing 48.91%. The interaction terms $I \times v$ and $I \times I$ contribute 29.67% and 13.02%, respectively, while U and v have contributions of 13.02% and 1.69% to D_{wb}. Fig. 8(b) to Fig. 8(d) show the interaction influence of process parameters on D_{wb}.

The correlation between the process parameters, including U, I, and v, and output characteristics such as W_{wb}, H_{wb}, and D_{wb} has been confirmed in several previous studies [14, 18]. Research shows that voltage and current significantly affect the W_{wb} and H_{wb}. Specifically, increasing the voltage typically leads to a greater weld width due to higher temperatures, while the current influences the weld height, which can either increase or decrease depending on specific conditions. To increase the weld width and height, the voltage can be raised, and the current can be adjusted accordingly. However, if a reduction in the D_{wb} is desired, reducing the v will increase the contact time with the material, thereby reducing penetration. These relationships emphasize the importance of optimizing process parameters to achieve desired characteristics in the welding process, while also improving the efficiency and quality of the surface coating.

3.3. Optimization results

Table 7 Solutions of optimization

Solution	U (V)	I (A)	v (m/min)	Fit W_{wb} (mm)	Fit H_{wb} (mm)	Fit D_{wb} (mm)	Composite desirability
1	22.0000	132.121	0.300000	0.544773	2.56572	5.06227	0.809781
2	22.0000	120.000	0.300000	0.408409	2.72990	4.56606	0.690246
3	21.2127	120.000	0.330071	0.494544	2.46544	4.40845	0.599427

In the context of optimization, composite desirability typically refers to a composite index used to measure the level of desirability of various responses or objectives based on multiple criteria. Composite desirability is used to evaluate how well a set of responses is optimized overall by the settings. Desirability has a range of zero to one. One represents the ideal case; zero indicates that one or more responses are outside their acceptable limits. The optimization results are shown in Table 7, where the three solutions with the highest composite desirability are indicated among all solutions.

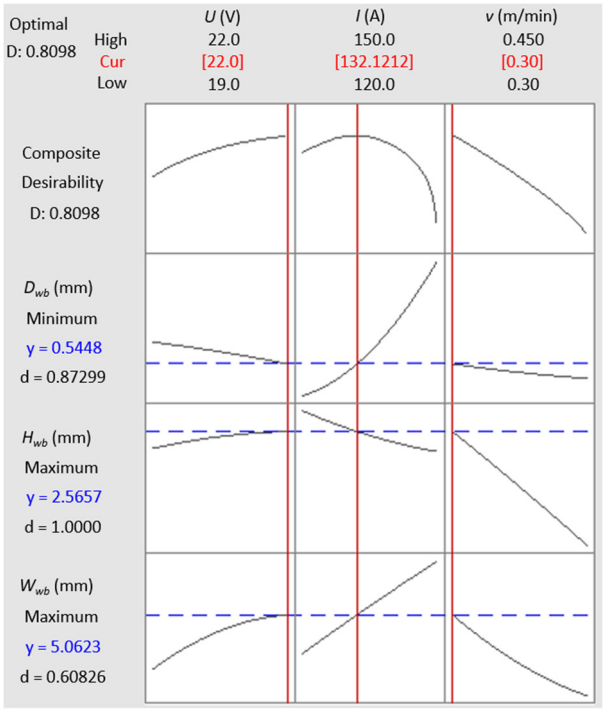

Fig. 9 Optimization plot

The solution to the multi-attribute optimization problem (Eq. (1)) is illustrated in Fig. 9. The optimal input variables are U = 22 V, I = 132 A, and v = 0.3 m/min. These parameters correspond to a composite desirability value of 0.8098 and predicted responses of W_{wb} = 5.06 mm, H_{wb} = 2.57 mm, and D_{wb} = 0.54 mm. Compared to the worst-case scenario (experiment run #13) where H_{wb} was minimum, the optimal parameters improved H_{wb} and W_{wb} by 56.71% and 25.87%, respectively, while reducing D_{wb} by 21.74% (Table 8). The obtained optimal parameters and resulting weld bead characteristics can generate toolpaths in coating SS309L on carbon steel surfaces, paving the way for applications in industries such as desalination, petrochemicals, and nuclear energy.

Table 8 Evaluation of optimal results

	Process parameters			Attributes		
	U (V)	I (A)	v (m/min)	W_{wb} (mm)	H_{wb} (mm)	D_{wb} (mm)
Exp. run 13	22	120	0.45	4.02	1.64	0.69
Optimal solution	22	132	0.3	5.06	2.57	0.54
Comparison	-	-	-	-25.87%	-56.71%	-21.74%

4. Conclusions

In this study, the influences of process parameters on single weld beads in the surface coating of SS309L by WAAM are investigated. The focus is placed on predicting how the process parameters (U, I, and v) influence the weld bead characteristics (including W_{wb}, H_{wb}, and D_{wb}), and on finding the proper process parameters for coating applications of WAAM. The key outcomes are summarized below:

(1) The torch movement speed v features the greatest impact on H_{wb} and W_{wb}, while I show the highest influence on D_{wb}. When U rises W_{wb} increases, while D_{wb} and H_{wb} decrease. Meanwhile, increasing I lead to a decrease in W_{wb} and H_{wb}. D_{wb} significantly increases as the current rises from 130 A to 150 A, with a slight increase in D_{wb} as the current continues to increase. Alternatively, increasing v leads to a reduction in W_{wb} and H_{wb}.

(2) The developed models of W_{wb}, H_{wb}, and D_{wb} exhibit acceptable accuracy, with R-squared values of 98.18%, 98.30%, and 98.19%, respectively. These models can predict the weld bead characteristic in WAAM of SS309L across the entire design space.

(3) The proper parameters for coating SS309L on carbon steel substrate using WAAM are I = 132 A, U = 22 V, and v = 0.3 m/min with a composite desirability value of 0.8098. The optimal parameters enhance H_{wb} and W_{wb} by 56.71% and 25.87%, respectively, while reducing D_{wb} by 21.74% compared to the worst-case scenario.

The results of this study can be utilized for future research, including investigations into the microstructure, mechanical properties, wear resistance, and corrosion resistance of SS309L coatings on carbon steel surfaces using WAAM. Additionally, these findings may be applied in various industries, such as desalination, petrochemical, and nuclear sectors.

Acknowledgments

This research is funded by the Le Quy Don Technical University Research Fund under the grand number “23.1.55”.

Conflicts of Interest

The authors declare no conflict of interest.

References

[1] I. S. Kim, J. S. Lee, and A. Kimura, “Embrittlement of ER309L Stainless Steel Clad by σ-Phase and Neutron Irradiation,” Journal of Nuclear Materials, vol. 329–333, part A, pp. 607-611, 2004.

[2] N. Switzner and Z. Yu, "Austenitic Stainless Steel Cladding Interface Microstructures Evaluated for Petrochemical Applications," Welding Journal, vol. 98, no. 2, pp. 50S-61S, 2019.
[3] J. W. Oldfield and B. Todd, "Technical and Economic Aspects of Stainless Steels in MSF Desalination Plants," Desalination, vol. 124, no. 1–3, pp. 75-84, 1999.
[4] S. W. Williams, F. Martina, A. C. Addison, J. Ding, G. Pardal, and P. Colegrove, "Wire + Arc Additive Manufacturing," Materials Science and Technology, vol. 32, no. 7, pp. 641-647, May 2016.
[5] P. Kazanas, P. Deherkar, P. Almeida, H. Lockett, and S. Williams, "Fabrication of Geometrical Features Using Wire and Arc Additive Manufacture," Proceedings of the Institution of Mechanical Engineers, Part B: Journal of Engineering Manufacture, vol. 226, no. 6, pp. 1042-1051, 2012.
[6] D. Ding, Z. Pan, D. Cuiuri, and H. Li, "Wire-Feed Additive Manufacturing of Metal Components: Technologies, Developments and Future Interests," The International Journal of Advanced Manufacturing Technology, vol. 81, no. 1-4, pp. 465-481, 2015.
[7] V. T. Le, D. S. Mai, T. K. Doan, and H. Paris, "Wire and Arc Additive Manufacturing of 308L Stainless Steel Components: Optimization of Processing Parameters and Material Properties," Engineering Science and Technology, an International Journal, vol. 24, no. 4, pp. 1015-1026, 2021.
[8] T. Zhao, H. Liu, L. Li, W. Liu, J. Yue, T. Wang, et al., "An Automatic Compensation Method for Improving Forming Precision of Multi-Layer Multi-Bead Component," Proceedings of the Institution of Mechanical Engineers, Part B: Journal of Engineering Manufacture, vol. 235, no. 8, pp. 1284-1297, 2021.
[9] J. Xiong, G. Zhang, J. Hu, and L. Wu, "Bead Geometry Prediction for Robotic GMAW-Based Rapid Manufacturing Through a Neural Network and a Second-Order Regression Analysis," Journal of Intelligent Manufacturing, vol. 25, no. 1, pp. 157-163, 2014.
[10] V. T. Le, D. S. Mai, V. T. Dang, D. M. Dinh, T. H. Cao, and V. A. Nguyen, "Optimization of Weld Parameters in Wire and Arc-Based Directed Energy Deposition of High Strength Low Alloy Steels," Advances in Technology Innovation, vol. 8, no. 1, pp. 01-11, 2023.
[11] S. Suryakumar, K. P. Karunakaran, A. Bernard, U. Chandrasekhar, N. Raghavender, and D. Sharma, "Weld Bead Modeling and Process Optimization in Hybrid Layered Manufacturing," Computer-Aided Design, vol. 43, no. 4, pp. 331-344, 2011.
[12] A. Kumar and K. Maji, "Selection of Process Parameters for Near-Net Shape Deposition in Wire Arc Additive Manufacturing by Genetic Algorithm," Journal of Materials Engineering and Performance, vol. 29, no. 5, pp. 3334-3352, 2020.
[13] F. Youheng, W. Guilan, Z. Haiou, and L. Liye, "Optimization of Surface Appearance for Wire and Arc Additive Manufacturing of Bainite Steel," The International Journal of Advanced Manufacturing Technology, vol. 91, no. 1-4, pp. 301-313, 2017.
[14] D. T. Sarathchandra, M. J. Davidson, and G. Visvanathan, "Parameters Effect on SS304 Beads Deposited by Wire Arc Additive Manufacturing," Materials and Manufacturing Processes, vol. 35, no. 7, pp. 852-858, 2020.
[15] N. Pravin Kumar, G. Sreedhar, S. Mohan Kumar, B. Girinath, A. Rajesh Kannan, R. Pramod, et al., "Microstructure and Electrochemical Evaluation of ER-308L Weld Overlays on AISI 321 Stainless Steel for Repair Applications," Proceedings of the Institution of Mechanical Engineers, Part E: Journal of Process Mechanical Engineering, vol. 238, no. 1, pp. 441-450, 2024.
[16] S. C. Bozeman, O. B. Isgor, and J. D. Tucker, "Effects of Processing Conditions on the Solidification and Heat-Affected Zone of 309L Stainless Steel Claddings on Carbon Steel Using Wire-Directed Energy Deposition," Surface and Coatings Technology, vol. 444, article no. 128698, 2022.
[17] D. Van Thuc, D. Van Luu, P. H. Cuong, Q. T. Ha, and T. D. Van, "Influence of WAAM Process Parameters on Morphology of Beads When Coating High-Temperature Stainless Steels SS309L on Low Carbon Steel Plates," International Research Journal of Advanced Engineering and Science, vol. 8, no. 2, pp. 183-186, 2023.
[18] V. T. Le, D. S. Mai, T. K. Doan, and Q. H. Hoang, "Prediction of Welding Bead Geometry for Wire Arc Additive Manufacturing of SS308l Walls Using Response Surface Methodology," Transport and Communications Science Journal, vol. 71, no. 4, pp. 431-443, 2020.
[19] D. S. Nagesh and G. L. Datta, "Prediction of Weld Bead Geometry and Penetration in Shielded Metal-Arc Welding Using Artificial Neural Networks," Journal of Materials Processing Technology, vol. 123, no. 2, pp. 303-312, 2002.
[20] S. Jindal, R. Chhibber, and N. P. Mehta, "Effect of Welding Parameters on Bead Profile, Microhardness and H2 Content in Submerged Arc Welding of High-Strength Low-Alloy Steel," Proceedings of the Institution of Mechanical Engineers, Part B: Journal of Engineering Manufacture, vol. 228, no. 1, pp. 82-94, 2014.